Appl. Phys. A (2016) 122:275
DOI 10.1007/s00339-016-9786-3

Applied Physics A
Materials Science & Processing

The characteristics of novel bimodal Ag–TiO_2 nanoparticles generated by hybrid laser-ultrasonic technique

Abubaker Hamad[1] · Lin Li[1] · Zhu Liu[2] · Xiang Li Zhong[2] · Grace Burke[2] · Tao Wang[3]

Received: 9 August 2015 / Accepted: 22 October 2015 / Published online: 7 March 2016

Abstract Silver–titania (Ag–TiO_2) nanoparticles with smaller Ag nanoparticles attached to larger TiO_2 nanoparticles were generated by hybrid ultrasonic vibration and picosecond laser ablation of Ag and Ti bulk targets in deionised water, for the first time. The laser has a wavelength of 1064 nm and a pulse duration of 10 ps. It was observed that without the ultrasonic vibration, Ag and TiO_2 nanoparticles did not combine, thus the role of ultrasonic vibration is essential. In addition, colloidal TiO_2 and Ag nanoparticles were generated separately for comparison under the same laser beam characteristics and process conditions. The absorption spectra of colloidal Ag–TiO_2 cluster nanoparticles were examined by UV–Vis spectroscopy, and size distribution was characterised using transmission electron microscopy. The morphology and composition of Ag–TiO_2 nanoparticles were examined using scanning transmission electron microscopy in high-angle annular dark field, and energy-dispersive X-ray spectroscopy. The crystalline structures were investigated by X-ray diffraction. The size of larger TiO_2 particles was in the range 30–150 nm, and the smaller-sized Ag nanoparticles attached to the TiO_2 was mainly in the range of 10–15 nm. The yield is more than 50 % with the remaining nanoparticles in the form of uncombined Ag and TiO_2. The nanoparticles generated had strong antibacterial effects as tested against *E. coli*. A discussion is given on the role of ultrasonic vibration in the formation of Ag–TiO_2 hybrid nanoparticles by picosecond laser ablation.

✉ Abubaker Hamad
abubaker.hamad75@yahoo.co.uk

[1] Laser Processing Research Centre, School of Mechanical, Aerospace and Civil Engineering, The University of Manchester, Manchester M13 9PL, UK

[2] School of Materials, The University of Manchester, Manchester M13 9PL, UK

[3] Faculty of Medical and Human Sciences, The University of Manchester, Manchester M13 9PL, UK

1 Introduction

The specific properties of nanoparticles which are different from bulk materials have received much attention over the last two decades [1], and nanoparticles have been used in a wide range of applications from electronic and catalytic uses to magnetic and medical fields [2]. The phases, size and shape of nanoparticles are responsible for the specific properties found in metal and metal oxide nanoparticles [3].

Both the hydrophilic and photocatalytic properties of TiO_2 nanoparticles are important for numerous applications, such as antimicrobial activity [4] and self-cleaning [5]. The photocatalytic activity of TiO_2 requires the activation with a UV light, which limits its applications. To overcome this limitation, the widely adopted method is to dope TiO_2 nanoparticles with other materials, such as transition metals [6] and non-metals [7].

Many methods have been developed not only for the preparation of nanoparticles but also to control their sizes. In general, the methods of nanoparticle generation can be divided into three types: chemical, physical and biological, amongst which are sol–gel, chemical vapour deposition (CVD), physical vapour deposition (PVD), wet chemistry, ion sputtering, plasma or flame pyrolysis [8], laser ablation of a solid metal in a liquid environment [9–12] and the use of Murraya Koenigii (curry leaf) extract [13].

Several methods and experimental set-ups have been proposed to combine Ag and TiO_2 nanoparticles and improve their properties; Guo et al. [14] prepared cage-bell

hybrid Ag-modified TiO_2 nanoparticles by means of an environmental template-free (alcoholysis) route followed by a facile impregnation (calcination). The photocatalytic activity of the particles was improved. Yang et al. [15] prepared hybrid Ag–TiO_2 core–shell nanoparticles by a chemical method which enhanced their photocatalytic activity in comparison with commercial TiO_2 and Ag-doped TiO_2 nanocomposite structures. Petronella et al. [16] prepared a composite of TiO_2 nanorods and Ag nanoparticles and succeeded in achieving the degradation of antibiotic nalidixic acid and a recalcitrant pollutant. Su et al. [17] combined the electrospinning technique with a solvo-thermal process to generate Ag/TiO_2 nanoheterostructures (Ag nanocrystals/TiO_2 nanofibre mats based) and showed an improvement in the properties of the particle's nanostructure. The product exhibits excellent photocatalytic activity for the degeneration of rhodamine B dye under visible light irradiation; Zhang et al. [18] used a laser beam to combine Ag/TiO_2 nanoparticles by laser ablation in liquid media and subsequent hydrothermal treatment without using any organic additive or chemical reduction agent. Firstly, colloidal TiO_x nanoparticles were produced from a bulk target by laser ablation in liquid (LAL), then they were mixed with different concentrations of $AgNO_3$ solution, and then it was put and kept in an electric oven at 180 °C for 1 day (24 h). It was claimed that the combination of Ag and TiO_2 using this method was stronger than other methods, as during the crystallisation process of TiO_x, silver ions were reduced and then deposited on the surface of TiO_2 nanoparticles. In our previous work, Hamad et al. [19], Ag–TiO_2 compound nanoparticles were produced via laser ablation in ice water. The energy gap of the TiO_2 nanoparticles was reduced significantly due to ice environment after doping with Ag nanoparticles. Although a combination between TiO_2 and Ag nanoparticles was observed, the yield was very low (approximately 5 %).

Recent decades have seen a growing interest in the use of laser ablation of a solid material target in a liquid environment as a technique for the preparation of nanoparticles [9, 10, 20], including porous nanoparticles [21], metal oxide nanoparticles [2], nanodisks [11], and for the morphological conversion of nanoparticles [22]. In comparison with chemical methods, colloidal nanoparticles prepared by laser ablation in a liquid environment are free from contamination [23], surfactants, counter-ions [11, 24, 25], and chemical reagents [1]. Furthermore, this method is a relatively simple way to prepare nanoparticles [26, 27] without the need for the removal of unwanted chemicals. With the generation of nanoparticles in deionised water, work has also been reported on preparing noble metal nanoparticles using sodium dodecyl sulphate (SDS) as a surfactant in a colloidal solution [9, 10, 28, 29] and a polyvinylpyrrolidone (PVP) solution [30, 31].

Nanoparticle clusters with smaller conducting nanoparticles attached to larger dielectric nanoparticles are desirable for many applications including antibacterial functions, light scattering control, local plasmonic tuning, and enhanced efficiency in thin film solar cells. In the present research, the authors present a new technique to combine two different nanoparticles using picosecond laser ablation of Ag and Ti solid targets in ultrasonic-assisted deionised water to achieve a single-step high yield in generating bimodal Ag and TiO_2 nanoparticle clusters.

2 Experimental materials and procedures

2.1 Materials

An Ag target plate with the dimensions of 25 mm (length) × 25 mm (width) × 2 mm (thickness) and a purity of 99.99 %, and a Ti target plate with the dimensions 25 mm (length) × 25 mm (width) × 1 mm (thickness) and a purity of 99.99 + % were used to generate the Ag–TiO_2 nanoparticles. Both targets were washed in autoclaved deionised water as well as in ethanol. The samples were then sonicated for 10–20 min in deionised water and ethanol before laser irradiation. They were placed in deionised water side by side (Fig. 1) during the laser ablation.

2.2 Preparation of Ag–TiO_2 nanoparticles by hybrid ultrasonic sonication and laser ablation

Ag–TiO_2 cluster nanoparticles were produced using the picosecond laser ablation in deionised water in an ultrasonic tank (Ultraschall-Reiniger, Emmi 5 with a power of 50 W at a pulse repetition rate of 49 kHz, tank volume 500 ml, digital timer 1–9 min adjustable). Ag and Ti plates

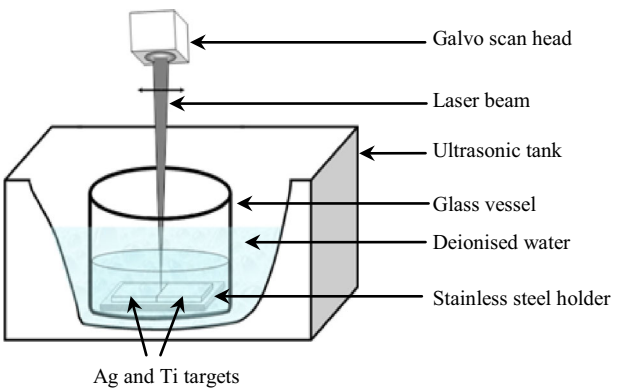

Fig. 1 Experimental set-up for generation of Ag–TiO_2 nanoparticles in deionised water in an ultrasonic cleaning bath

Table 1 400 W edgewave picosecond laser beam parameters used to produce Ag–TiO_2 cluster nanoparticles

Parameters	Value
Wavelength (λ)	1064 nm
Frequency (f)	200 kHz
Laser beam power (P)	9.12 W
Scan speed (v)	250 mm/s
Laser pulse duration (τ)	10 ps
Laser post size in diameter (D)	125 μm
Laser pulse energy (E_{pulse})	45.6 μJ
Laser fluence (F_{laser})	0.37 J/cm^2

were put on a sample holder, beside each other, in a glass vessel containing about 20 ml of deionised water. Then the glass vessel was put in an ultrasonic tank filled with deionised water. The deionised water in the glass vessel was poured to a level of about 2 mm above the samples. The laser ablation experimental set-up is shown in Fig. 1. It should be noted that the effect of the water level on the laser beam focal length was taken into account. Under the same laser conditions and experimental set-up (with ultrasonic-assisted production), TiO_2 nanoparticles were generated to show whether single nanoparticles would combine or not. For comparison, Ag and Ag–TiO_2 nanoparticles were generated under the same laser beam parameters and experimental conditions without ultrasonic vibration. Table 1 shows laser beam parameters used in this work.

To identify the optimal laser beam parameters to produce nanoparticles in deionised water, several sets of laser beam powers and scan speeds were examined. The optimal laser parameters for preparation of Ag–TiO_2 nanoparticles are shown in Tables 2 and 3.

The morphology of nanoparticles in all cases was spherical. The number of larger nanoparticles at the 50 mm/s scan speed was a little higher in comparison at 250 mm/s and the ablation rate at 9.12 W was higher than that at 5.9 W. As shown in Tables 2 and 3, the smallest average nanoparticles were obtained at 9.12 W average power and 250 mm/s scan speed. Although smaller nanoparticles of <10 nm were also observed, these were in very small quantities.

2.3 Nanoparticle sample preparation for characterisation

For TEM analysis, a drop of the colloidal suspension of nanoparticles was deposited onto a copper microgrid mesh (A Formvar/Carbon on 200 copper mesh) and then allowed to dry in ambient air temperature. This process was repeated three to six times to ensure that the sufficient amount of nanoparticles was collected on the copper mesh substrate. The concentration of the colloidal nanoparticle samples was obtained by measuring the weight of the targets before and after the nanoparticle generation process using a microbalance scale. The X-ray diffraction sample was prepared on a glass slide; firstly the produced colloidal nanoparticles were centrifuged for 10–15 min using a microcentrifuge machine, then they were dropped onto the glass slide and allowed to dry in ambient air. This process was repeated several times to deposit a sufficient amount of nanoparticles on the slide.

2.4 Characterisation

In order to characterise the nanoparticles, a UV–Vis spectrometer (Analytic Jena, SPECORD 250, dual beam) was used for examining the absorption spectra of the colloidal nanoparticles. A transmission electron microscope (TEM) (JEOL 2000 FX AEM) was used to examine the morphology of the nanoparticles and measure their sizes and size distribution. Images and composition of Ag–TiO_2 nanoparticles were obtained using scanning transmission electron microscope (STEM) where high-angle annular dark field (HAADF) imaging was employed for the examination of the morphology of the nanoparticles and energy-dispersive X-ray spectroscopy (EDS) line scan was used to analyses the chemical composition. The morphological characterisations were examined by a field-emission gun transmission electron microscope (FEI Tecnai G^2 F30). In addition, X-ray diffraction (XRD) was used for the investigation of crystalline material structures. A microbalance scale (Sartorius BL 210S) with a resolution of 0.1 mg was used to measure the weight of the samples before and after ablation process, and the concentration of the colloidal nanoparticles was calculated after measuring the amount of deionised water.

2.5 Antibacterial activity test procedure

The antibacterial activities of the nanoparticles were examined against *E. coli* bacteria (JM109 from Promega, UK). A single colony of *E. coli* (or 10 μl of glycerol stock) was incubated in 10 ml of lysogeny broth (LB broth) in a 50-ml tube and cultured at 37 °C overnight with constant shaking at 225 rpm. The optical density of the cultured *E. coli* was measured at 600 nm (OD_{600}) and diluted down to a colony-forming unit (CFU)/ml of about 8×10^4 with LB. 200 μl of colloidal nanoparticles was mixed with 1.80 ml of the diluted *E. coli* and incubated for 6 h at 37 °C while shaking at 225 rpm. Finally, 10 μl of each dilution was spread on the LB agar plates and left at room temperature for about 48 h under normal light followed by

Table 2 Optimal laser parameters at constant laser power $P(60\ \%) = 9.12$ W and different scan speeds

Scan speed (mm/s)	Size distribution (nm)	Ablation rate (mg/min)	Average size (nm)
50	10–200	0.073	42.5
150	10–230	0.060	50.5
250	10–200	0.056	35.5
2000	10–250	0.08	44

Table 3 Optimal laser beam parameters at constant scan seed (250 mm/s) and different laser power

Laser power (W)	Size distribution (nm)	Ablation rate (mg/min)	Average size (nm)
3.36	10–290	0.026	71
5.95	10–200	0.053	43.5
9.12	10–200	0.056	35.5

counting colonies on each plate. For negative control, 200 µl of nanoparticles was replaced by 200 µl dH_2O.

3 Results

3.1 Ag–TiO_2 nanoparticle characteristics

Figure 2 shows the optical absorption spectra of the Ag, TiO_2 and Ag–TiO_2 nanoparticles (with and without ultrasonic vibration) generated by a picosecond laser in deionised water. Two different materials, Ag and TiO_2, contributed to the formation of the Ag–TiO_2 spectrum. The Ag nanoparticles spectrum has two peaks: the first is a weak absorption peak in the range of 200–250 nm, which is formed due to inter-band transition, and the second is a strong transition peak located around 410 nm formed due to surface plasmon resonance [1]. The optical absorption spectra of the Ag–TiO_2 nanoparticles produced with and without ultrasonic vibration (Fig. 2b) indicate that there is no shift of the surface plasmon peak position both at 404 nm. Another spectrum in the figure is the TiO_2 absorption spectrum that can be divided into two regions: the UV region, which has a higher absorption rate than the visible region. The absorption rate in the UV region decreases sharply when approaching the visible region. As shown in Fig. 2, the Ag–TiO_2 absorption spectra have a strong peak in the UV range, which is almost exactly the same as with the TiO_2 band, and the second peak in the visible range is formed due to the surface plasmon resonance of the Ag nanoparticles because pure Ag has a strong peak at this wavelength which is about 400 nm. The general shape of Ag–TiO_2 nanoparticle optical absorption spectra depends on the ratio of ablated Ag and TiO_2 nanoparticles in the solution. For example, when the amount of ablated Ag nanoparticles is increased, the surface plasmon resonance (SPR) peak will become higher, which is an indication that the Ag concentration in the solution has increased. However, when the amount of TiO_2 nanoparticles is increased a strong peak at 200–250 nm appears. It was noted that the amount of ablated nanoparticles in the solution rose with prolonged irradiation time.

In terms of morphology, size and size distribution, there is no significant difference between the Ag–TiO_2 nanoparticles produced with and without ultrasonic vibration except that combination of Ag and TiO_2 nanoparticles (i.e. smaller Ag nanoparticles were attached to the larger

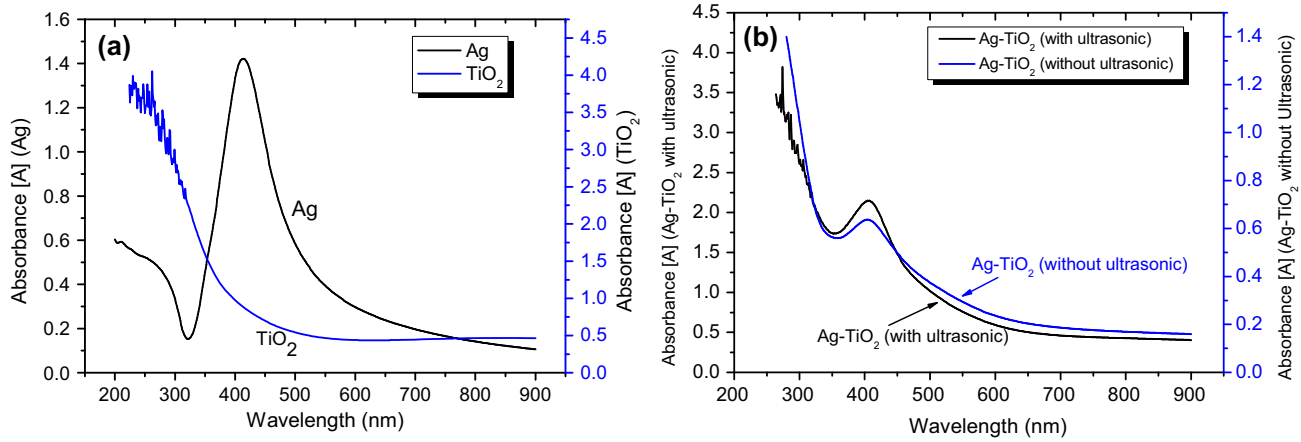

Fig. 2 Absorption spectra of **a** Ag, TiO_2 and **b** Ag–TiO_2 colloidal nanoparticles generated in deionised water in an ultrasonic tank and without ultrasonic tank by picosecond laser ablation in deionised water ($P = 9.12$ W, $f = 200$ kHz and $v = 250$ mm/s). In the Ag–TiO_2 suspension produced in the ultrasonic tank, the amount of Ag and TiO_2 nanoparticles were 0.5 mg and 0.6 mg, respectively. The ablation time for Ag, TiO_2 and Ag–TiO_2 with ultrasonic waves was 16 min, and for Ag–TiO_2 without ultrasonic waves it was 10 min

TiO_2 nanoparticles) occurred in the case of having the ultrasonic vibrations in the nanoparticle production process.

Figures 3a–d show the TEM images of the Ag–TiO_2 nanoparticles generated in deionised water in an ultrasonic bath. Spherical Ag–TiO_2 nanoparticles of different sizes are produced. The weight ratio of Ag–TiO_2 nanoparticles was 1:1.2, so the amount of TiO_2 nanoparticles was 20 % higher than the amount of Ag nanoparticles. Figure 3e shows a histogram of the size distribution of 612 of the produced Ag–TiO_2 nanoparticles; the distribution is between few nanometres to 150 nm with an average size of 39 nm and a small amount of particles in the range of >150 nm up to 190 nm. The size distribution shape is lognormal distribution. Almost all of the large particles were TiO_2 particles and most of the small nanoparticles were Ag. As can be seen in the figure, a combination of the TiO_2 and Ag nanoparticles was formed. It is worth mentioning that the combination of two different nanoparticles by pure laser technique without using any chemical assistants such as organic additives or reduction agents or additional heating was not observed in the previous studies. The yield of the bimodal Ag–TiO_2 cluster was about 50 %.

Figure 4 shows the images of the bimodal Ag–TiO_2 nanoparticles recorded by the high-angle annular dark field microscope (HAADF). The combination of the Ag and TiO_2 nanoparticles appears clearly. Small silver nanoparticles in the range of 3–15 nm were deposited on the surface of larger (30–120 nm) TiO_2 particles. In addition, Fig. 4b reveals the existence of ultrafine nanoparticles on the surface of the TiO_2 particles, measuring a few nanometres.

Figure 5 shows the line scanning of the energy-dispersive X-ray spectroscopy (EDS) images of the Ag–TiO_2 nanoparticles formed by the picosecond laser ablation in deionised water with ultrasonic vibration. These images confirm the production of Ag and TiO_2 nanoparticles, which shows that the large particles are TiO_2 particles and the small nanoparticles are Ag. It can be concluded that the amount of Ti is higher than the amount of Ag and O compositions.

X-ray diffraction analysis was used for the determination of both the structure and crystal phase. Figure 6 shows the X-ray diffraction patterns of both the Ag and TiO_2 (or Ag–TiO_2) nanoparticles. The group of diffraction peaks, which include $2\theta = 38$, 44.4, 52, 76.75, 93.4 and 99

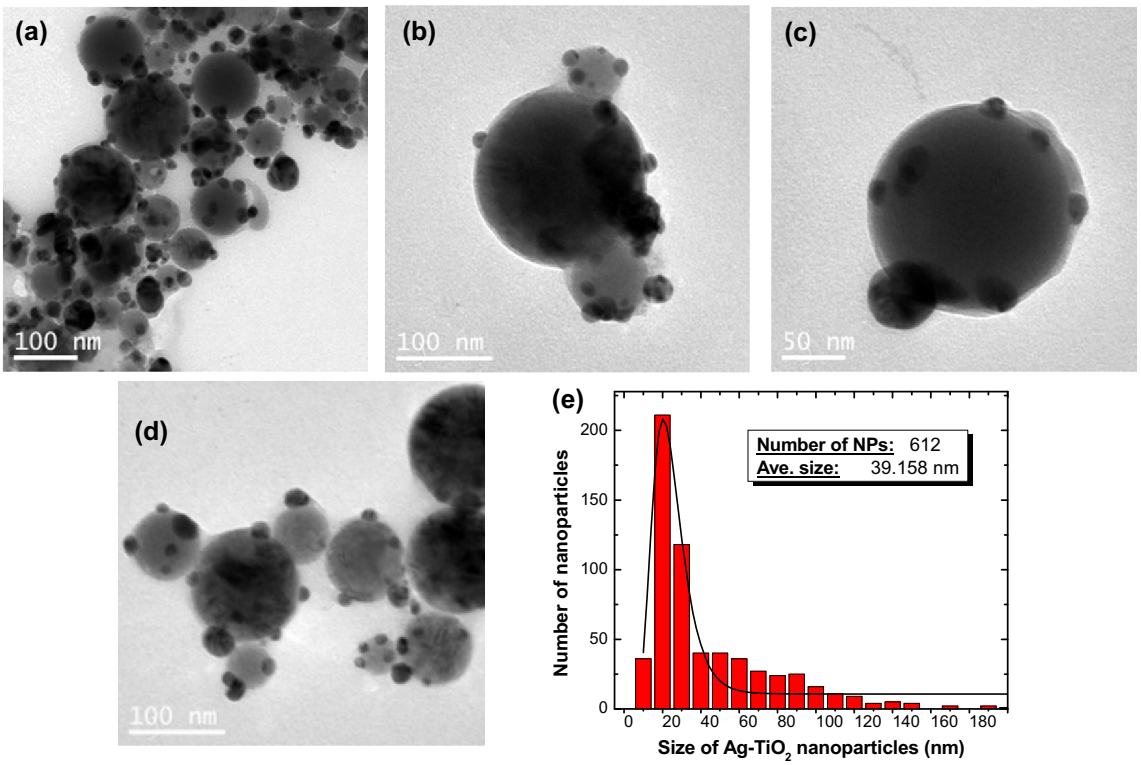

Fig. 3 **a–d** TEM images of Ag–TiO_2 nanoparticles generated in deionised water by the picosecond laser ($P = 9.12$ W, $f = 200$ kHz, $v = 250$ mm/s and $t = 16$ min). The production process was carried out in a tank of ultrasonic cleaner with a frequency 49 kHz. The ablation rate of Ag–TiO_2 nanoparticles was 0.068 mg/min with a Ag:TiO_2 ratio of 1:1.2. **e** Is the lognormal size distribution of Ag–TiO_2 nanoparticles

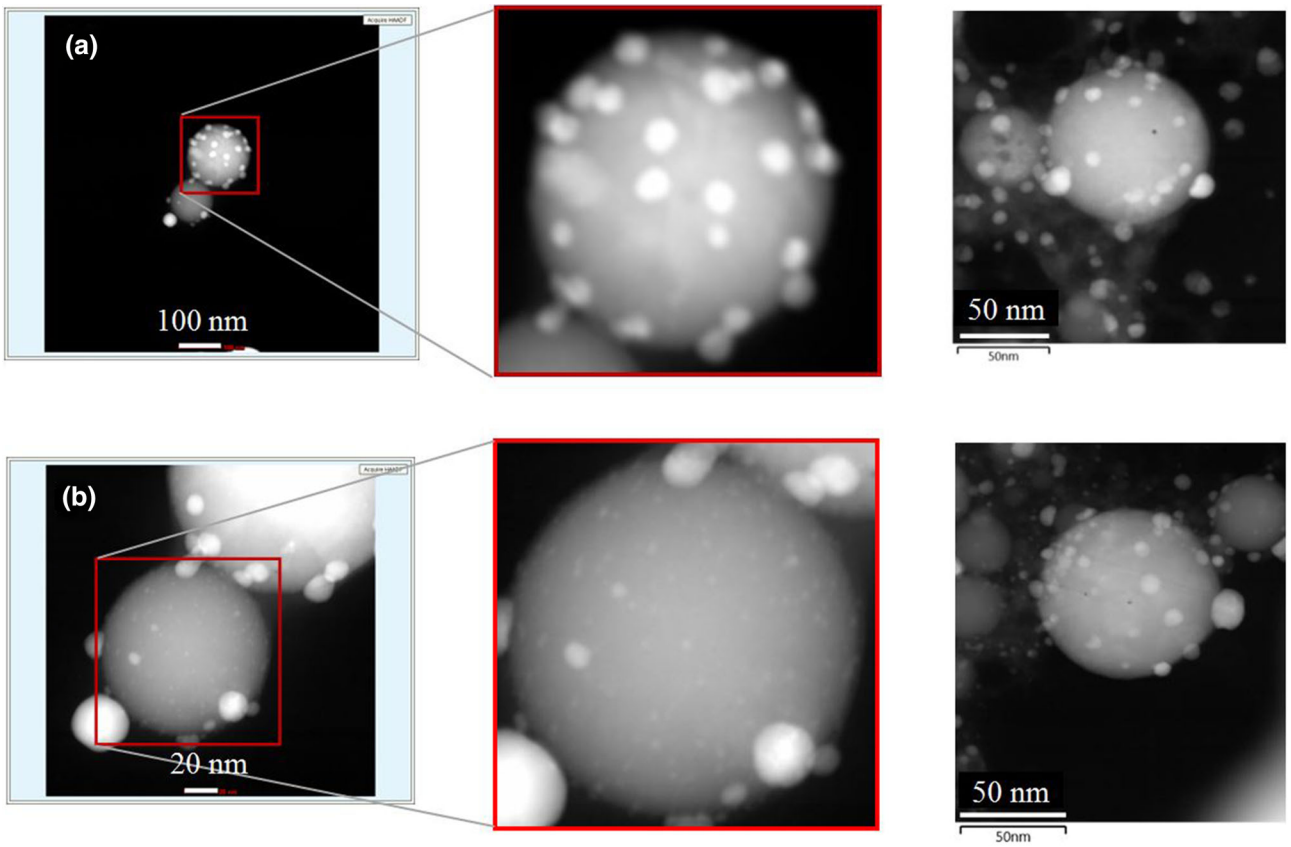

Fig. 4 High-angle annular dark field microscope (HAADF) images of the Ag–TiO_2 nanoparticles

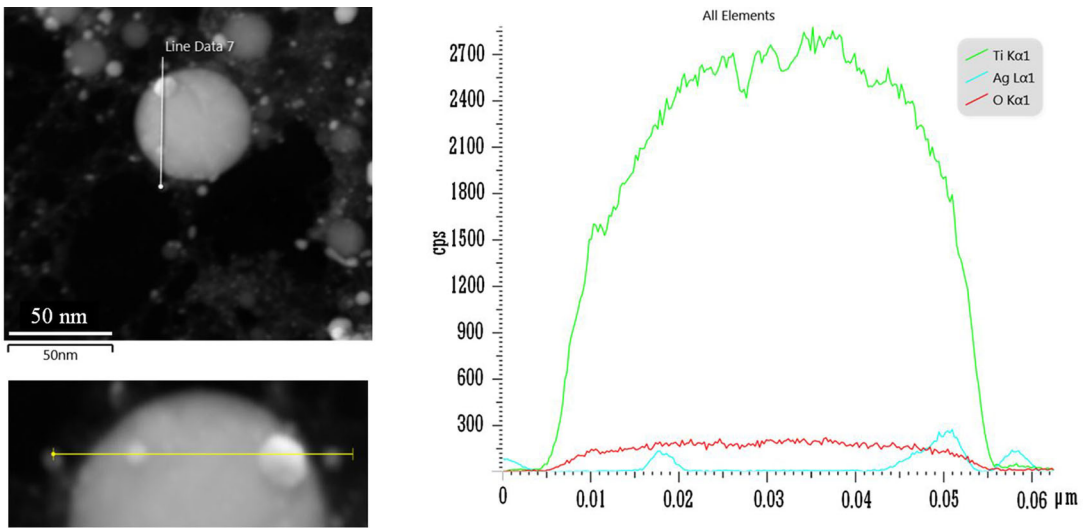

Fig. 5 EDS—line profile images of the Ag–TiO_2 nanoparticles synthesised by picosecond laser in deionised water supporting ultrasound waves in an ultrasonic cleaner

correspond to the Ag nanoparticles, and another group that includes $2\theta = 32$, 42, 48.2, 64 correspond to the rutile structure of the TiO_2 nanoparticles. In addition, a diffraction peak at $2\theta = 37.5$ corresponds to the existence of AgO. A previously published paper indicated that the peaks at $2\theta = 37.5$ and 48.1 were related to the existence

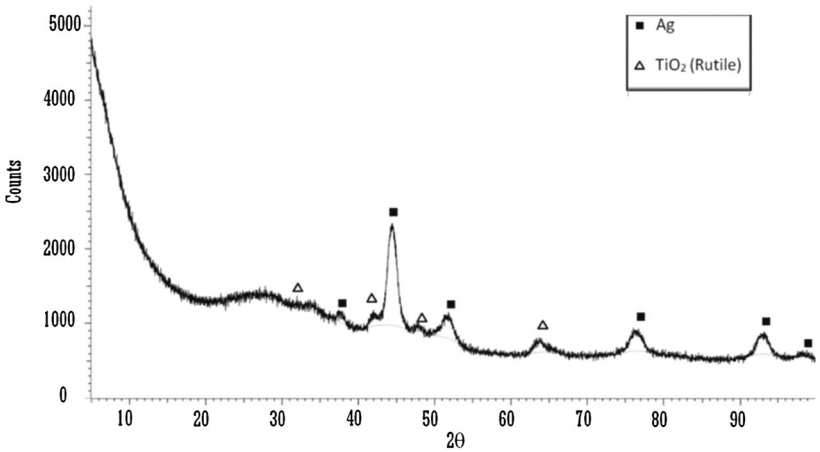

Fig. 6 X-ray diffraction (XRD) spectrum of Ag–TiO_2 nanoparticles produced by picosecond laser in deionised water in ultrasonic vibration

of anatase TiO_2 nanoparticles (annealed at 500 °C), which correspond to the 004 and 200 crystalline plains, respectively [32].

3.2 Ag–TiO_2 nanoparticles generation without ultrasonic vibration

Figure 7 shows the TEM images of Ag and TiO_2 nanoparticles fabricated by laser ablation in deionised water without using ultrasonic vibration. It was generated under the same laser beam conditions and experimental set-up but without ultrasonic vibration. It can be seen there is no clear combination between Ag and TiO_2 nanoparticles.

3.3 The characteristics of TiO_2 nanoparticles generated with ultrasonic vibration

In order to show whether this combination of nanoparticles would occur between the nanoparticles of single material or not, the TiO_2 nanoparticles were synthesised in deionised water in an ultrasonic bath. As shown in Fig. 8a, b, the TiO_2 nanoparticles did not combine. This is a valid proof that the combined particles that form the Ag–TiO_2 nanoparticles are the Ag and TiO_2 particles. The histogram image in Fig. 8c shows the size distribution of the TiO_2 nanoparticles, which indicates that the size distribution of the TiO_2 nanoparticles is wider than that of the Ag–TiO_2 nanoparticles; in other words, the large nanoparticles in the Ag–TiO_2 nanoparticles are TiO_2. The size distribution ranges from 10 nm to 140 nm, and a few other large particles above 140 nm are also evident.

3.4 The characteristics of laser-generated Ag nanoparticles

Ag nanoparticles synthesised by picosecond laser ablation in deionised water without ultrasonic vibration. As shown in Fig. 9a, b, semi-spherical Ag nanoparticles were produced. The particle size histogram graph (Fig. 9c) shows the size distribution of silver nanoparticles ranged from about 2 nm to about 100 nm. The average size of 660 counted nanoparticles was 32.5 nm. It was fabricated to show and compare their antibacterial activity with ultrasonic-assisted Ag–TiO_2 hybrid nanoparticles.

3.5 Antibacterial characteristics

Figure 10 shows the antibacterial activity of Ag–TiO_2 nanoparticles (produced with ultrasonic vibration) under standard room light with the weight ratio 1:1.2 which were tested against *E. coli* bacteria (JM109 from Promega, UK) and compared with Ag and TiO_2 nanoparticles, and with non-nanoparticle control. The nanoparticles at a concentration 20 μg/ml demonstrate significant antibacterial activity.

It is worth noting that the Ag concentration within the bimodal Ag–TiO_2 nanoparticles is much less than that in pure Ag nanoparticle solution, while the antibacterial activity is similar, indicating that TiO_2 in this combined form has played a role in antibacterial activity.

The antibacterial activity of TiO_2 nanoparticles produced by the picosecond laser in deionised water without using ultrasonic vibration was examined against *E. coli* bacteria with the same concentration 20 μg/ml. The results show that the antibacterial activity of the Ag–TiO_2 nanoparticles is much better than that of the TiO_2 nanoparticles.

Figure 11 shows the relationship between the concentration of the Ag–TiO_2 cluster nanoparticles (generated with ultrasonic assisted) and the number of survived bacteria after co-culturing with Ag–TiO_2 nanoparticles. The results were also compared with the effect of Ag nanoparticles. It can be seen that the number of surviving bacteria is decreased by increasing the concentration of the

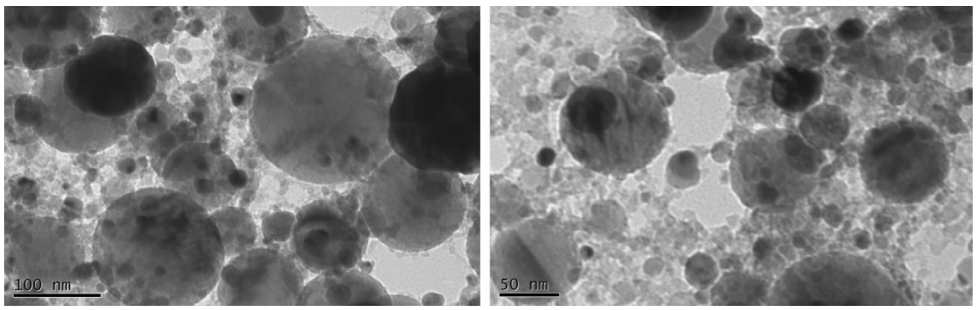

Fig. 7 TEM images of Ag–TiO_2 nanoparticles produced in deionised water using picosecond laser without using ultrasonic waves (wavelength 1064 nm, power 9.12 W, frequency 200 kHz and scan speed 250 mm/s and $t = 10$ min)

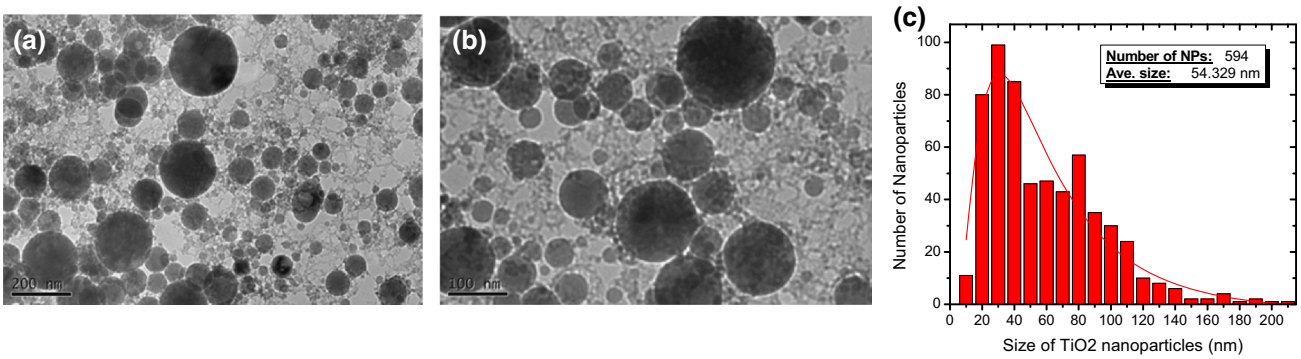

Fig. 8 **a**, **b** TEM images of TiO_2 nanoparticles generated in deionised water in an ultrasonic cleaner tank by picosecond laser ($P = 9.12$ W, $f = 200$ kHz, $v = 250$ mm/s and $t = 15$ min). The quantity of TiO_2 nanoparticles generated in the suspension is 0.8 mg and the concentration is 53.3 μg/ml. The ablation rate of TiO_2 NPs is 0.0533 mg/min. (0.8 mg/15 min). **c** Histogram of the size distribution of TiO_2 nanoparticles

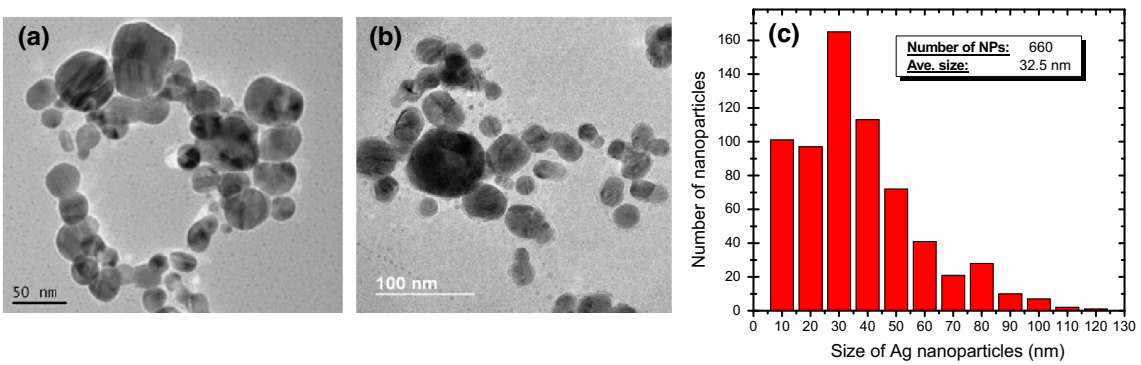

Fig. 9 **a**, **b** TEM images of Ag nanoparticles generated by picosecond laser in deionised water without ultrasonic vibration. Laser parameters are $P = 9.12$ W, $f = 200$ kHz, $v = 250$ mm/s. **c** Histogram of the size distribution of Ag nanoparticles

nanoparticles for both the Ag–TiO_2 and Ag nanoparticles. At each nanoparticle concentration, the number of survived *E. coli* in Ag nanoparticles was significantly lower (higher bacterial killing effect) than that of Ag–TiO_2 nanoparticles, but the ratio of the Ag nanoparticles to Ag–TiO_2 nanoparticles is 1:1.2 which is lower than the amount of Ag nanoparticles. Pure Ag nanoparticles could eliminate all bacteria at 20 μg/ml. It can be expected that the Ag–TiO_2 nanoparticles will be able to kill a full *E. coli* bacteria colony at a higher concentration.

4 Discussion

4.1 Generation of Ag–TiO_2 cluster and TiO_2 nanoparticles

The first sign of the generation of Ag–TiO_2 nanoparticles is a change in the colour of the deionised water or the contamination of the deionised water by the generated nanoparticles. The second sign of the presence of these nanoparticles can be observed by noting the absorption

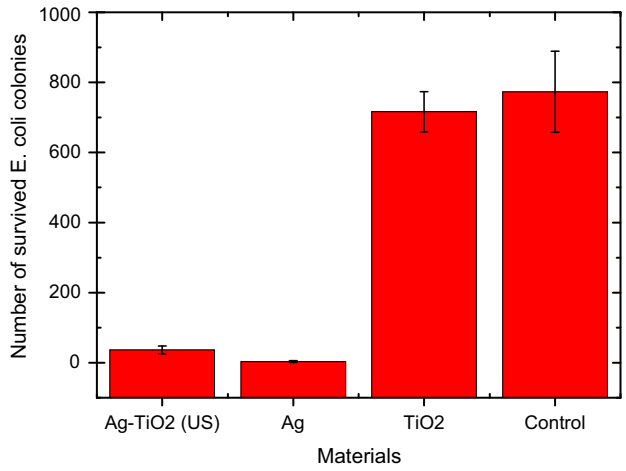

Fig. 10 Antibacterial activity of Ag–TiO_2 nanoparticles in comparison with control sample. Equal amount of *E. coli* were cultured with [Ag–TiO_2 (ultrasonic wave based generation), Ag and TiO_2] nanoparticles or without (control) nanoparticles in LB broth for 6 h and 10 µl of the broth culture was plated on to LB agar plate for colony formation after overnight incubation at 37 °C overnight. The number of *E. coli* colonies represents the survived *E. coli* after culturing with or without nanoparticles which negatively correlate to the antibacterial effect of the nanoparticles

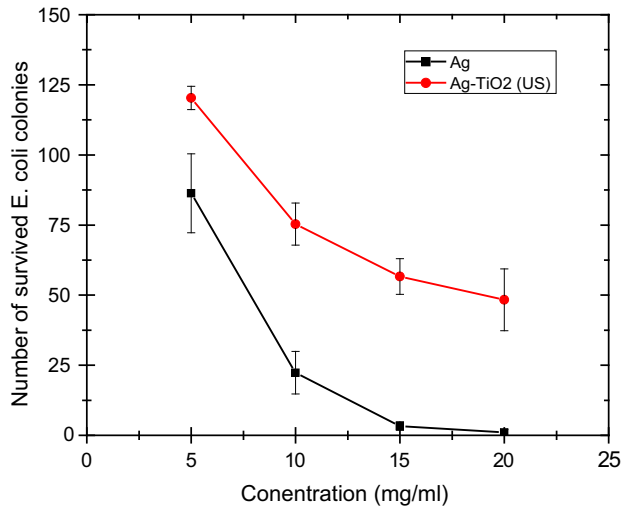

Fig. 11 Relationship between the number of surviving *E. coli* bacteria as a function of the concentration of Ag–TiO_2 (US) (ultrasonic) and Ag nanoparticles generated by picosecond laser in deionised water with ultrasonic wave assisted. The antibacterial test was carried out under normal light

spectra of the generated colloidal nanoparticles. When the laser beam is incident on the surface of the target, firstly, the laser beam interacts with the deionised water. Because water has a significant absorption coefficient, some power of the laser beam will be lost. The amount of power absorbed by the water can be calculated according to Lambert's law.

$$I = I_o e^{-\alpha x} \quad (1)$$

where I and I_o are the transmitted and incident intensity of the laser beam, respectively, α is the absorption coefficient of the deionised water and x is the height of the water level above the samples. The water level covering the target material has an effect not only on the laser beam power or intensity but also on the laser beam focal length [33]. For example, the amount of laser power loss for a 2 mm of water level above the target is about 4 %; this amount will be increased to 8 % when the water level is 4 mm above the bulk target, so there is a linear relationship between the water height and laser power loss. As well as for a 2 mm water level, the distance between the target and the focusing lens should be increased by an extra 0.5 mm and for 4 mm of water an extra 1 mm [33, 34]. In this work, the effects of both cases were considered.

It is worth mentioning that some water will be lost through evaporation during the generation of nanoparticles by ablation. The amount of evaporated water on a sunny day on which the maximum temperature is 20 °C and the minimum is 9 °C and using a picosecond laser under the same laser beam parameters which are used for the generation of nanoparticles can be found using the following equation:

$$y = 0.0505t + 0.0499 \quad (2)$$

where y is the amount of evaporated deionised water and t is time. For example after 10 min the amount of evaporated water will be 0.55 g/10 min. (0.055 g/min).

After laser–water interaction, laser–target and water–target interactions will occur when the laser beam strikes the surface of the target or at the water–target interface. At this point, shock waves in the target material and another shock wave in the water will be produced and propagated [35]. This is may be due to Newton's third law (action and reaction).

A spark plume was produced at the water–matter interface; the plume was shiny and looks like a small flame. When the laser energy is equal to or greater than the ablation threshold of the target material, the ablation process will begin, followed by the production of nanoparticles through the condensation of the target material vapour. After observing the nanoparticle production process using a digital camera, it was discovered that the generated nanoparticles were propagated along the laser beam axis from the target surface to the water–air interface inside the solution. This occurred due to a decrease in the density of the solution along the beam path (see Fig. 12).

TiO_2 nanoparticles were generated immediately after the production of Ti vapour in the solution and then interacted with water. As a result, titanium(IV) hydroxide ($Ti(OH)_4$)

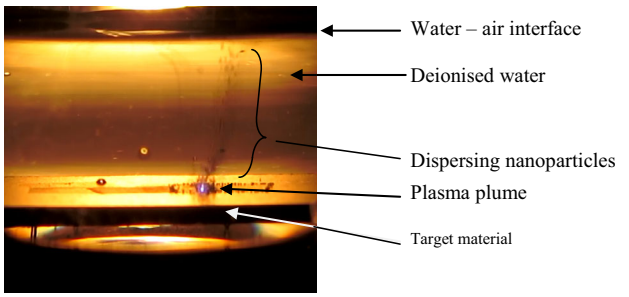

Fig. 12 Image of plasma plume and nanoparticles dispersing in deionised water during picosecond laser ablation of a target (without using ultrasonic waves). The photograph is taken after recording the ablation process by a normal camera

was produced, followed by the production of TiO_2 nanoparticles according to the Eqs. (3) and (4) [36].

$$Ti(\text{clusters}) + H_2O \rightarrow Ti(OH)_4 + H_2 \uparrow \quad (3)$$

$$Ti(OH)_4 \rightarrow TiO_2 + H_2O \quad (4)$$

As shown in Table 2, the ablation rate of the nanoparticles is decreased with an increase in scan speed at the lower scan speeds (50, 150 and 250 mm/s) because when the nanoparticles were dispersed in the solution they would travel towards the laser (see Fig. 12). As a result, they would scatter the laser beam and prevent the laser from reaching the target. This would lead to less nanoparticles produced from the target material. However, the ablation rate at a higher scan speed (2000 mm/s) is increased slightly in comparison at 50 mm/s scan speed, this is because at higher scan speed more laser power will reach the target per unit time in comparison with that at a low scan speed. Although the minimum size of the nanoparticles was observed at the 250 mm/s scan speed, the fluctuation of the size and size distribution was observed. This may be due to the presence of a liquid level on the target material since large size particles would be generate due to liquid layer ejection and fragmentation [37]. As such the actual water level on the target in one experiment may not be exactly the same as in another experiment.

In general, the optical absorption spectra of the Ag–TiO_2 nanoparticles produced with and without ultrasonic vibration have the same features. The surface plasmon resonance is higher than that produced without ultrasonic waves. This is because the amount of the Ag nanoparticles is higher with the ultrasonic waves due to longer exposure time.

4.2 Ag and TiO_2 combination

In the present research, hybrid ultrasonic vibration and laser ablation was used to generate and modify Ag–TiO_2 cluster nanoparticles for the first time. Ultrasound waves have been used in many applications such as measuring distance, defect recognition within an object, detecting the presence of objects, imaging (sonography) and cleaning devices (ultrasonic cleaners). Ultrasonic cleaning devices can be classified into traditional ultrasonic and megasonic frequencies, as their working frequencies are in the range of 20 kHz–500 kHz and 0.5 MHz–5 MHz, respectively. When ultrasonic waves disperse into the solution, they create compression waves, consequently rupturing the solution and generating an enormous number of voids or cavities. These huge quantities of bubbles collapse and produce very high temperature and pressure that is 5000 K and 20,000 lbs/inch^2, respectively [38, 39]. These very high temperatures increase the Brownian motion and mobility of the surface atoms; as a result, collisions between nanoparticles will increase, followed by adhesion and coalescence between them [40]. The combination between Ag and TiO_2 nanoparticles was not observed while producing them without ultrasonic vibration because in the case of absent ultrasonic vibration the high pressure and temperature will not be generated.

Several mechanisms have been provided to explain production of nanoparticles by laser ablation in deionised water [37, 41]. In general, generation of nanoparticles in a liquid environment by laser ablation can be divided into two steps: firstly, generation of nanoparticles from the target material and secondly, dispersion of nanoparticles in the liquid media. As observed experimentally, the size and size distribution of the Ag–TiO_2 nanoparticles were quite similar when they are produced with and without ultrasonic vibration. The only difference between them is the combination of the Ag with the TiO_2 nanoparticles.

The ultrasound interaction with matter depends on the characteristic of the ultrasonic wave, type of the material, and the physical properties of the material such as acoustic impedance. Acoustic impedance measure the resistance of the material to mechanical vibration [42]. In addition, higher ultrasonic power density or higher frequency leads to the increased effects of the ultrasonic waves on the materials. At a fixed ultrasonic power and frequency, the denser nanoparticles are more affected by ultrasonic waves. Here, Ag nanoparticles were more affected by ultrasonic power than the lower density TiO_2. As a result, the Ag nanoparticles were directed or moved to attach the lighter TiO_2 nanoparticles. The ultrasonic waves act as a driving force to combine different nanoparticles in liquid media because of the acoustic wave properties such as density, sound speed, and specific acoustic impedance which are different in air, water, and even in different materials. In addition, for a sinusoidal ultrasonic wave of rms acoustic pressure amplitude at 100 Pa, the particle velocity amplitude, displacement amplitude, and acceleration amplitude are different at different frequencies [43]. When ultrasonic

wave interacts with a solid material, its amplitude will be decreased in the material due to absorption or scattering which means that the some energy will be absorbed by nanoparticles which leads to a change in their direction which acts as a driving force [44]. Here, it can be said that the ultrasonic waves might have not effected the generation mechanism of nanoparticles such as phase transition, thermodynamic, and kinetic growth, but they have an effect on the combination of two different types of nanoparticles while they are still hot (during the laser ablation) that have different physical properties. In addition, ultrasonic waves were used to dismantle large-sized particles to small-sized particles [45] and to disperse agglomerated nanoparticles in deionised water [46].

4.3 Antibacterial activity

The antibacterial activity of nanoparticles depends on the types of nanoparticles, such as Ag, Au, or TiO_2. In addition, the concentration and the amount of nanoparticles used for antibacterial tests are two important factors for eliminating microorganisms. It is worth mentioning that the antimicrobial efficiency will be increased by increasing the concentration and the amount of nanoparticles in the solution to a certain extent. This increases the efficacy of the solution, because in both cases the number of nanoparticles in the solution will be increased, and as a result the chance of bacteria coming into contact with the nanoparticles will be increased leading to killing more numbers of bacteria. It is worth mentioning that the concentration of both Ag and Ag–TiO_2 cluster nanoparticles was 20 μg/ml, but the amount Ag in the Ag–TiO_2 cluster nanoparticles was less than half (Ag–TiO_2 weight ratio of 1:1.2) in comparison with the pure Ag nanoparticles, expecting less toxicity to human cells (our separate work, to be published, on the comparison of toxicity of Ag–TiO_2 cluster with Ag nanoparticles shows that Ag nanoparticles tend to penetrate into the human cells while the Ag–TiO_2 clusters tend to remain outside the human cells), despite that the antibacterial activity of pure Ag nanoparticles was a little higher than Ag–TiO_2 cluster nanoparticles.

5 Conclusions

Bimodal Ag–TiO_2 cluster nanoparticles were generated using a hybrid ultrasonic sonication and picosecond laser ablation in deionised water. The method has allowed the attachment of smaller Ag particles onto the larger TiO_2 nanoparticles with a yield of approximately 50 %. This method has been demonstrated for the first time. The results show that there is no combination between Ag and TiO_2 nanoparticles produced in deionised water without ultrasonic vibration. In addition, the combination is not obtained between TiO_2 nanoparticles upon placing them in the ultrasonic machine. This method is a new way of combining two different nanoparticles.

The Ag–TiO_2 cluster nanoparticles have good antibacterial activity and this activity is enhanced by increasing the concentration and amount of nanoparticles in the solution.

References

1. T. Tsuji, K. Iryo, N. Watanabe, M. Tsuji, Preparation of silver nanoparticles by laser ablation in solution: influence of laser wavelength on particle size. Appl. Surf. Sci. **202**(1–2), 80–85 (2002)
2. Z. Liu, Y. Yuan, S. Khan, A. Abdolvand, D. Whitehead, M. Schmidt, L. Li, Generation of metal-oxide nanoparticles using continuous-wave fibre laser ablation in liquid. J. Micromech. Microeng. **19**(5), 054008 (2009)
3. T. Tsuji, Y. Okazaki, T. Higuchi, M. Tsuji, Laser-induced morphology changes of silver colloids prepared by laser ablation in water: enhancement of anisotropic shape conversions by chloride ions. J. Photochem. Photobiol., A **183**(3), 297–303 (2006)
4. K. Gupta, R. Singh, A. Pandey, A. Pandey, Photocatalytic antibacterial performance of TiO_2 and Ag-doped TiO_2 against *S. aureus*. *P. aeruginosa* and *E. coli*. Beilstein. J. Nanotechnol. **4**(1), 345–351 (2013)
5. L. Graziani, E. Quagliarini, F. Bondioli, M. D'Orazio, Durability of self-cleaning TiO_2 coatings on fired clay brick façades: effects of UV exposure and wet & dry cycles. Build. Environ. **71**, 193–203 (2014)
6. X.-X. Xue, W. Ji, Z. Mao, Z.-S. Li, Z.-N. Guo, B. Zhao, C. Zhao, SERS study of Co-doped TiO_2 nanoparticles. Chem. Res. Chin. Univ. **29**(4), 751–754 (2013)
7. C. Burda, Y. Lou, X. Chen, A.C. Samia, J. Stout, J.L. Gole, Enhanced nitrogen doping in TiO2 nanoparticles. Nano Lett. **3**(8), 1049–1051 (2003)
8. S. Khan, Y. Yuan, A. Abdolvand, M. Schmidt, P. Crouse, L. Li, Z. Liu, M. Sharp, K.G. Watkins, Generation and characterization of NiO nanoparticles by continuous wave fiber laser ablation in liquid. J. Nanopart. Res. **11**(6), 1421–1427 (2009)
9. F. Mafuné, J.-Y. Kohno, Y. Takeda, T. Kondow, H. Sawabe, Structure and stability of silver nanoparticles in aqueous solution produced by laser ablation. J. Phys. Chem. B **104**(35), 8333–8337 (2000)
10. F. Mafuné, J.-Y. Kohno, Y. Takeda, T. Kondow, H. Sawabe, Formation and size control of silver nanoparticles by laser ablation in aqueous solution. J. Phys. Chem. B **104**(39), 9111–9117 (2000)
11. A.V. Simakin, V.V. Voronov, G.A. Shafeev, R. Brayner, F. Bozon-Verduraz, Nanodisks of Au and Ag produced by laser ablation in liquid environment. Chem. Phys. Lett. **348**(3–4), 182–186 (2001)

12. T. Tsuji, T. Kakita, M. Tsuji, Preparation of nano-size particles of silver with femtosecond laser ablation in water. Appl. Surf. Sci. **206**(1–4), 314–320 (2003)
13. P. Singh, R.B. Raja, Biological synthesis and characterization of silver nanoparticles using the fungus *Trichoderma harzianum*. Asian J. Exp. Biol. Sci. **2**, 600–605 (2011)
14. H. Guo, W. Wang, L. Liu, Y. He, C. Li, Y. Wang, Shape-controlled synthesis of Ag@ TiO_2 cage-bell hybrid structure with enhanced photocatalytic activity and superior lithium storage. Green Chem. **15**(10), 2810–2816 (2013)
15. X. Yang, H. Fu, K. Wong, X. Jiang, A. Yu, Hybrid Ag@ TiO_2 core–shell nanostructures with highly enhanced photocatalytic performance. Nanotechnology **24**(41), 415601 (2013)
16. F. Petronella, S. Diomede, E. Fanizza, G. Mascolo, T. Sibillano, A. Agostiano, M. Curri, R. Comparelli, Photodegradation of nalidixic acid assisted by TiO_2 nanorods/Ag nanoparticles based catalyst. Chemosphere **91**(7), 941–947 (2013)
17. C. Su, L. Liu, M. Zhang, Y. Zhang, C. Shao, Fabrication of Ag/TiO_2 nanoheterostructures with visible light photocatalytic function via a solvothermal approach. CrystEngComm **14**(11), 3989–3999 (2012)
18. H. Zhang, C. Liang, J. Liu, Z. Tian, G. Wang, W. Cai, Defect-mediated formation of ag cluster-doped TiO_2 nanoparticles for efficient photodegradation of pentachlorophenol. Langmuir **28**(8), 3938–3944 (2012)
19. A. Hamad, L. Li, Z. Liu, X.L. Zhong, T. Wang, Picosecond laser generation of Ag–TiO_2 nanoparticles with reduced energy gap by ablation in ice water and their antibacterial activities. Appl. Phys. A **119**(4), 1387–1396 (2015)
20. Y.-H. Chen, C.-S. Yeh, Laser ablation method: use of surfactants to form the dispersed Ag nanoparticles. Colloids Surf. A **197**(1–3), 133–139 (2002)
21. P.G. Kuzmin, G.A. Shafeev, G. Viau, B. Warot-Fonrose, M. Barberoglou, E. Stratakis, C. Fotakis, Porous nanoparticles of Al and Ti generated by laser ablation in liquids. Appl. Surf. Sci. **258**(23), 9283–9287 (2012)
22. T. Tsuji, Y. Okazaki, M. Tsuji, Photo-induced morphological conversions of silver nanoparticles prepared using laser ablation in water—enhanced morphological conversions using halogen etching. J. Photochem. Photobiol., A **194**(2–3), 247–253 (2008)
23. B. Fei, Z. Xin-Zheng, W. Zhen-Hua, W. Qiang, H. Hao, X. Jing-Jun, Preparation and size characterization of silver nanoparticles produced by femtosecond laser ablation in water. Chin. Phys. Lett. **25**(12), 4463 (2008)
24. S.I. Dolgaev, A.V. Simakin, V.V. Voronov, G.A. Shafeev, F. Bozon-Verduraz, Nanoparticles produced by laser ablation of solids in liquid environment. Appl. Surf. Sci. **186**(1–4), 546–551 (2002)
25. P.V. Kazakevich, A.V. Simakin, V.V. Voronov, G.A. Shafeev, Laser induced synthesis of nanoparticles in liquids. Appl. Surf. Sci. **252**(13), 4373–4380 (2006)
26. T.X. Phuoc, Y. Soong, M.K. Chyu, Synthesis of Ag-deionized water nanofluids using multi-beam laser ablation in liquids. Opt. Lasers Eng. **45**(12), 1099–1106 (2007)
27. T. Tsuji, T. Hamagami, T. Kawamura, J. Yamaki, M. Tsuji, Laser ablation of cobalt and cobalt oxides in liquids: influence of solvent on composition of prepared nanoparticles. Appl. Surf. Sci. **243**(1–4), 214–219 (2005)
28. T. Sasaki, C. Liang, W.T. Nichols, Y. Shimizu, N. Koshizaki, Fabrication of oxide base nanostructures using pulsed laser ablation in aqueous solutions. Appl. Phys. A **79**(4–6), 1489–1492 (2004)
29. C.H. Liang, Y. Shimizu, T. Sasaki, N. Koshizaki, Preparation of ultrafine TiO_2 nanocrystals via pulsed-laser ablation of titanium metal in surfactant solution. Appl. Phys. A **80**(4), 819–822 (2005)
30. T. Tsuji, D.H. Thang, Y. Okazaki, M. Nakanishi, Y. Tsuboi, M. Tsuji, Preparation of silver nanoparticles by laser ablation in polyvinylpyrrolidone solutions. Appl. Surf. Sci. **254**(16), 5224–5230 (2008)
31. T. Tsuji, T. Mizuki, S. Ozono, M. Tsuji, Laser-induced silver nanocrystal formation in polyvinylpyrrolidone solutions. J. Photochem. Photobiol., A **206**(2–3), 134–139 (2009)
32. J.-J. Park, D.-Y. Kim, J.-G. Lee, Y.-H. Cha, M.T. Swihart, S.S. Yoon, Supersonic aerosol-deposited TiO_2 photoelectrodes for photoelectrochemical solar water splitting. RSC Adv. **4**(17), 8661–8670 (2014)
33. Z. Yan, D.B. Chrisey, Pulsed laser ablation in liquid for micro-/nanostructure generation. J. Photochem. Photobiol., C **13**(3), 204–223 (2012)
34. A. Menéndez-Manjón, P. Wagener, S. Barcikowski, Transfer-matrix method for efficient ablation by pulsed laser ablation and nanoparticle generation in liquids. J. Phys. Chem. C **115**(12), 5108–5114 (2011)
35. T.E. Itina, On nanoparticle formation by laser ablation in liquids. J. Phys. Chem. C **115**(12), 5044–5048 (2010)
36. S.M. Hong, S. Lee, H.J. Jung, Y. Yu, J.H. Shin, K.-Y. Kwon, M.Y. Choi, Simple preparation of anatase TiO_2 nanoparticles via pulsed laser ablation in liquid. Bull. Korean Chem. Soc. **34**(1), 4 (2013)
37. M.E. Povarnitsyn, T.E. Itina, P.R. Levashov, K.V. Khishchenko, Mechanisms of nanoparticle formation by ultra-short laser ablation of metals in liquid environment. Phys. Chem. Chem. Phys. **15**(9), 3108–3114 (2013)
38. A. Henglein, M. Gutierrez, Sonochemistry and sonoluminescence: effects of external pressure. J. Phys. Chem. **97**(1), 158–162 (1993)
39. L. Azar, Cavitation in ultrasonic cleaning and cell disruption. Control. Environ. 14–17. www.cemag.us
40. A. Amarjargal, L. Tijing, C. Kim, One-pot synthesis of silver–titanium dioxide nanocomposites using ethylene glycol medium and their antibacterial properties. Dig. J. Nanomater. Biostruct. **6**(4), 1957–1965 (2011)
41. N.G. Semaltianos, S. Logothetidis, N. Frangis, I. Tsiaoussis, W. Perrie, G. Dearden, K.G. Watkins, Laser ablation in water: a route to synthesize nanoparticles of titanium monoxide. Chem. Phys. Lett. **496**(1–3), 113–116 (2010)
42. N.M. Tole, H. Ostensen, *Basic Physics of Ultrasonographic Imaging* (World Health Organization, Geneva, 2005)
43. T.G. Leighton, What is ultrasound? Prog. Biophys. Mol. Biol. **93**(1), 3–83 (2007)
44. W.D. O'Brien, Ultrasound–biophysics mechanisms. Prog. Biophys. Mol. Biol. **93**(1), 212–255 (2007)
45. B. Bittmann, F. Haupert, A.K. Schlarb, Ultrasonic dispersion of inorganic nanoparticles in epoxy resin. Ultrason. Sonochem. **16**(5), 622–628 (2009)
46. J.S. Taurozzi, V.A. Hackley, M.R. Wiesner, Ultrasonic dispersion of nanoparticles for environmental, health and safety assessment-issues and recommendations. Nanotoxicology **5**(4), 711–729 (2011)